Preparation and Characterization of Conductive and Photoluminescent DNA-Templated Polyindole Nanowires

Reda Hassanien,[†] Mariam Al-Hinai,[‡] Said A. Farha Al-Said,[†] Ross Little,[§] Lidija Šiller,[§] Nicholas G. Wright,[‡] Andrew Houlton,[†] and Benjamin R. Horrocks[†,*]

[†]Chemical Nanoscience Laboratories, School of Chemistry, Bedson Building, [‡]School of Electrical, Electronic and Computing Engineering, and [§]School of Chemical Engineering and Advanced Materials, Newcastle University, Newcastle Upon Tyne NE1 7RU, United Kingdom

ABSTRACT Polyindole (PIn) nanowires were formed on a λ-DNA template by chemical oxidation of indole using aqueous FeCl$_3$. The resulting nanowires are smooth, regular, conductive and had diameters in the range of 5−30 nm. These features allow them to be aligned by molecular combing and studied by scanned conductance microscopy, conductive AFM, and two-terminal $I-V$ measurements. Using this combination of measurements, we find that the conductivity of PIn/DNA nanowires is between 2.5 and 40 S cm^{-1} at room temperature, which is substantially greater than that in previous reports on the bulk polyindole conductivity (typically $10^{-2}-10^{-1}$ S cm^{-1}). The conductance at zero bias shows an Arrhenius-type of dependence on temperature over the range of 233 to 373 K, and the values observed upon heating and cooling are repeatable within 5%; this behavior is consistent with a hopping mechanism of conductivity.

KEYWORDS: conducting polymer · DNA · nanowires · polyindole · template synthesis · temperature dependence

The fabrication of nanometer-scale structures by chemical means is an active and technically important field.[1] DNA is an attractive molecule for use in nanofabrication because it is chemically robust, has highly specific recognition properties, and is available in precisely controlled lengths. These properties also make DNA a promising template on which to synthesize a range of organic and inorganic materials.[2] In a template synthesis approach to the preparation of nanowires, the length and the diameter of the resulting wires can be controlled by the length of the template and the reaction conditions. Although the inherent conductivity of DNA remains a matter of debate,[3,4] it is now generally accepted that long (μm) DNA molecules have low conductance. For this reason, a number of groups have coated DNA with materials such as metals,[5−9] semiconductors,[10−12] and conductive polymers.[13−15] Conductive polymers are simple to template on DNA because the oxidative polymerization conditions naturally produce the doped, positively charged form of the polymer; the nascent oligomers are therefore strongly attracted to a polyanion such as DNA. DNA/polymer nanowires also tend to show a smoother morphology than DNA-templated metals, but their conductivity is much lower.[14] Nevertheless, polymer nanowires are of interest because of the possibility to chemically functionalize the nanowire using simple methods of organic synthesis to derivatize the monomer[16] or to incorporate novel properties through the choice of the basic monomer unit.

Polyindole (PIn) and its derivatives have been investigated for applications in sensing and electronics and because they are photoluminescent as well as conductive polymers.[17,18] PIn can be obtained by electrochemical oxidation of indole in various electrolytes and by chemical polymerization using oxidants such as FeCl$_3$. The chemical and electrochemical syntheses of PIn have been discussed in detail.[19−26] Previous studies on the electrical properties of bulk PIn have reported a wide range of conductivities; some values have been as low as 0.03 mS cm^{-1},[22] and others in the range of 5 × 10^{-3} to 8 × 10^{-1} S cm^{-1}.[19,23] These variations most likely reflect differences in doping level, defect density, and structural factors. Recently, Eraldemir and co-workers reported the conductivity of chemically synthesized PIn, using FeCl$_3$ as the oxidant, to be 9.64 × 10^{-3} S cm^{-1}.[24]

In this study, we demonstrate a method for preparing DNA-templated polyindole (PIn/DNA) nanowires by chemical oxidation of the indole monomer using FeCl$_3$ as the oxidizing agent in the presence of a λ-DNA template at room temperature. The structural properties and the chemical composition of the PIn/DNA nanowires were characterized by means of Fourier transform

infrared (FTIR) spectroscopy, UV−vis spectroscopy, and X-ray photoelectron spectroscopy (XPS). The morphology and electrical properties of the resulting wires were investigated using atomic force microscopy (AFM), scanned conductance microscopy (SCM), and conductive atomic force microscopy (c-AFM). A new c-AFM procedure was developed in which electrical contact to individual polymer nanowires is made by a combination of molecular combing and drop-coating nanowire dispersions. This facilitated c-AFM measurements of nanowire resistance, and by determining the resistance as a function of distance along the nanowire, we have been able to distinguish the nanowire resistance from the possible contributions of the contacts. Temperature-dependent two-terminal current−voltage measurements at microfabricated Au electrodes were also performed to investigate the conduction mechanism and demonstrate the thermal stability of the polymer nanowires.

RESULTS AND DISCUSSION

Polymerization of Indole in DNA-Containing Solutions. Polyindole (PIn) nanowires were formed by chemical polymerization of indole using FeCl₃ as an oxidant in the presence of λ-DNA as template. Templating conductive polymers on DNA relies on the noncovalent interaction of the nascent polymer chains with the template. The material isolated from these reactions contains both cationic PIn and anionic DNA polymers. Intimate interaction of the two polymer chains in the self-assembled nanowires is indicated by FTIR and UV−vis spectroscopy. Moreover, AFM images provide a convenient method to observe the polymerization *via* changes in the thickness of the DNA strands as they become coated with conductive polymer.

Fourier Transform Infrared Spectroscopy. FTIR spectra were used to characterize the polymerization of indole and the interaction of PIn with λ-DNA. FTIR spectra of the product material provided evidence of the formation of a supramolecular hybrid polymer containing λ-DNA and PIn. The infrared spectra related to this discussion are presented in Figure 1. The study of PIn by FTIR spectroscopy has been described previously.[27] The strong, narrow peak at 3407 cm⁻¹ observed in the indole spectrum is characteristic of the N−H stretching mode; this peak becomes broad and shifts to 3275 cm⁻¹ in the PIn spectrum.[28]

The band at 745 cm⁻¹ in indole is typically assigned to out-of-plane C−H deformations on the benzene ring because it is also present in 2,3-disubstituted indoles. It is also present, with inhomogeneous broadening, in the PIn spectrum, and therefore, it is considered that polymerization does not involve coupling *via* the benzene ring.[21,25,29] The structure of polyindole is more complex than that of other conductive polymers, such as polypyrrole, because a number of different coupling
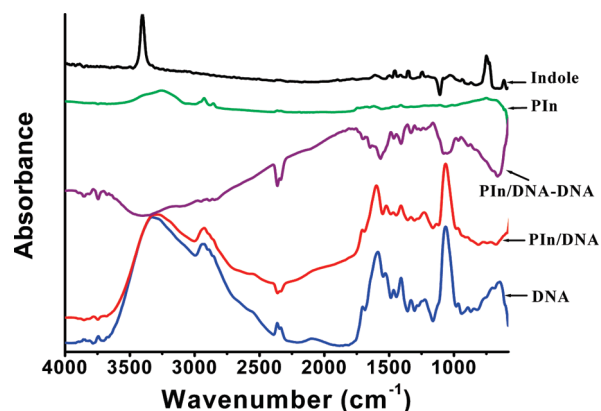

Figure 1. Transmission FTIR spectra of PIn/DNA *vs* controls. Spectra of indole (black), polyindole (PIn; green), λ-DNA (DNA; blue), PIn/DNA nanowires (red), and the difference spectrum (PIn/DNA−DNA; purple) are shown. The spectra are offset for clarity.

schemes are possible involving the 1-, 2-, and 3-positions.[25] It has also been shown that various polyindoles consist of linked cyclic trimer structures using laser-desorption laser-ionization time-of-flight mass spectrometry and electrochemical rotating ring-disk experiments.[26] We cannot determine the precise coupling of our PIn/DNA nanowires from FTIR data because the FTIR spectrum of the nanowires is substantially different than that of normal PIn.

In the PIn/DNA spectrum, broad intense bands due to bound water in DNA are present, although the negative feature in the difference spectrum (PIn/DNA−DNA) at 3300 cm⁻¹ shows that bound water has been displaced upon interaction of PIn with DNA. The presence of DNA in the PIn/DNA is revealed clearly in the 1000−2000 cm⁻¹ region, and the spectra of both DNA itself and the DNA-templated polymer are similar in this region, though a careful examination of the fingerprint region reveals that some of the DNA-related bands are slightly shifted relative to the pure DNA spectrum (Supporting Information). In particular, there is a shift of +8 cm⁻¹ upon PIn templating in the asymmetric stretch of the phosphate group. The strong, broad feature comprising components due to C═N vibrations in the nucleobases and bending vibrations of bound water is also shifted to higher wavenumber (1597 cm⁻¹) in PIn/DNA compared to 1585 cm⁻¹ in the DNA spectrum. The former suggests a quite expected interaction of the cationic polyindole with the phosphate groups, but the lat-
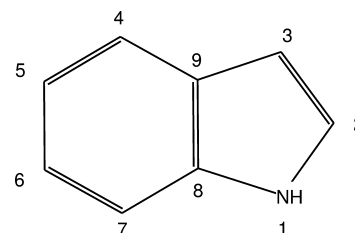
Scheme 1. Indole: oxidative polymerization of indole using FeCl₃ (aqueous) has been reported to involve coupling of monomers *via* the 1-, 2-, or 3-positions.
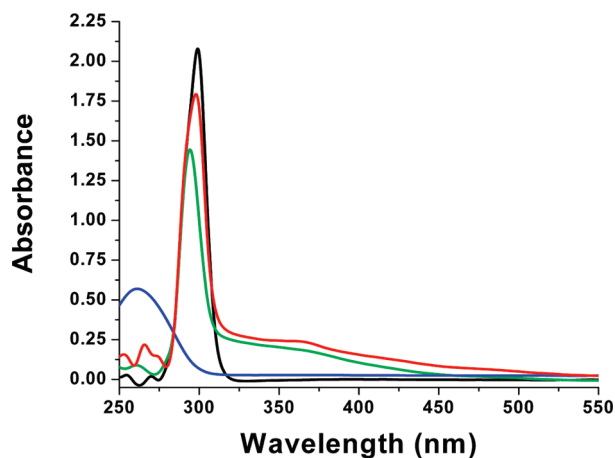
Figure 2. UV–vis absorption spectra of 6.24 mM indole (black), PIn (green), CT-DNA (blue), and PIn/DNA (red).

ter also indicates the PIn/DNA interaction is sufficiently intimate to affect the nucleobases. In summary, the FTIR spectra indicate that the PIn/DNA sample is not a simple mixture of DNA and PIn but rather an intimate interaction of DNA with PIn in the hybrid polymer in a similar manner to our previous report for polypyrrole/DNA nanowires.[14]

UV–Vis Absorption Spectroscopy. The UV–vis absorption spectra of indole, PIn, calf thymus (CT) DNA, and PIn/DNA recorded at room temperature in aqueous solution are shown in Figure 2.

Figure 2 shows the UV absorption spectrum of a freshly prepared solution of indole; three peaks at 255, 270, and 300 nm are observed. The PIn spectrum (stable with time for 14 days) also has a large peak at 296 nm and a smaller peak at 263 nm; these peaks correspond to n–π* and π–π* transitions of the polymer chain, respectively.[24] PIn/DNA solutions show a combination of these peaks due to the presence of some unreacted monomer, but there is also an increased absorption in the UV region where CT-DNA has a characteristic broad absorption band at 260 nm, and the peak positions are slightly shifted compared to PIn. In addition, the PIn and PIn/DNA spectra have a peak at about 370 nm and substantial tails extending into the visible region; these aspects of the spectra are very similar to previous reports for polyindole.[30] These features are not present in the monomer but are characteristic of this type of polymer and originate from the extended conjugation and the midgap states in the doped polymer formed during oxidative polymerization.

X-ray Photoelectron Spectroscopy. XPS survey spectra of PIn/DNA samples revealed the presence of the elements C, N, O, Cl, and (weakly) P. The N_{1s} and C_{1s} spectra of PIn/DNA samples examined in this study are presented in Figure 3. Three main peaks are observed in the N_{1s} spectrum of

PIn/DNA (Figure 3a). Previous workers have observed two components in the N_{1s} spectra of DNA alone: the lower binding energy component at 398.8 eV and another at 400.6 eV. The lower energy peak is attributed to neutral nitrogen atoms (e.g., the N atoms of the exocyclic amines). The component at 400.6 eV is observed for peptidic N atoms and is also typical of the N atoms in the pyrimidines of DNA.[31,32] While it is likely that the two lowest energy peaks in the N_{1s} spectra of PIn/DNA contain similar contributions from the DNA, there will also be a contribution to these features from the N atoms of polyindole according to the extent of protonation and doping level. This is consistent with previous reports on polyindole[29] and polypyrrole[33] in which it was proposed that the higher binding energy components are due to nitrogen atoms that bear a positive charge and are in chemically or structurally inequivalent environments. In summary, the N_{1s} peaks at 398.8 and 400.6 eV are typical of both polyindole and DNA. However, the third feature at 402.5 eV in our spectra is definitely not present in N_{1s} spectra of DNA and can be assigned to polyindole alone. N_{1s} spectra of polypyrrole have similarly been reported to contain a major peak at 400.6 eV and a higher binding energy signal at 402.5 eV; these were attributed to ($-NH^+$ (polaron)) and ($=NH^+$ (bipolaron)), respectively.[34] We therefore assign the third component in our PIn/DNA samples, with a binding energy of 402.5 eV, to positively charged nitrogen atoms associated with the charge carriers in PIn.

The C_{1s} spectra (Figure 3b) can be resolved into four different components centered at 284.4, 285.9, 287.3, and 289.0 eV. Four components have also been observed in C_{1s} spectra of pure DNA by previous workers, although the peak at 284.4 eV is dominant in pure DNA.[31] We assign the two components at the lowest binding energy to C–H, C–C, and C–N species from PIn and DNA. The third peak at 287.3 eV is attributed to carbons in functional groups of the type, C=N or C–N$^+$, mainly from PIn because this feature is more intense relative to the 285.9 and 284.4 eV components in our samples than in pure DNA.[31] Since the fourth
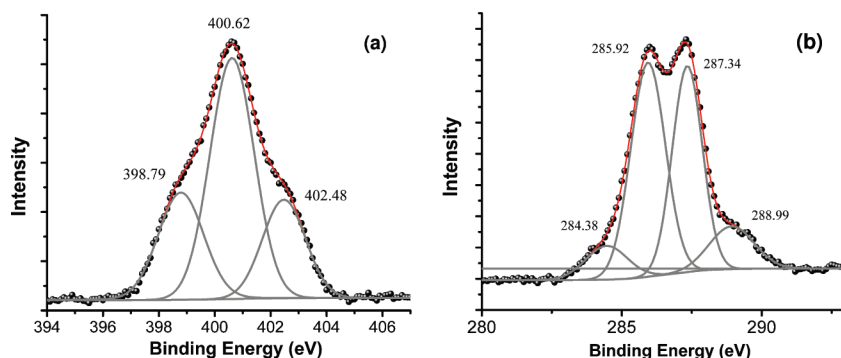

Figure 3. Core level XPS spectra of PIn/DNA: (a) N_{1s} spectrum and (b) C_{1s} spectrum. Peak positions of the fitted components are indicated.

peak at 289.0 eV is comparable to that at 284.4 eV in our samples, but is very weak in pure DNA,[31] we assign it to C≡N$^+$ carbons in PIn. In general, the XPS spectra of PIn/DNA show large contributions from species assigned to PIn, and in combination with the UV−vis absorption spectra, this indicates that the PIn/DNA nanowires should be visualized as a thick coat of PIn on the DNA template rather than a small number of PIn chains wrapping around the DNA. Chloride ions make up the required counter charge. The AFM images presented below are in general agreement with this picture of the PIn/DNA samples.

Atomic Force Microscopy of PIn/DNA Cast on Si/SiO$_2$ Surfaces. Previously, we have reported changes in the morphology of polypyrrole nanowires upon standing in the polymerization solution.[13] In that work, individual nanowires were found to combine together to form ropes, and these changes were visible in AFM images of drop-cast nanowires on mica or oxidized Si surfaces. The number density of nanowires on the substrate was controlled by adjusting the hydrophobicity of the substrate by increasing the extent of silanization: hydrophobic surfaces favored the observation of individual wires, and hydrophilic surfaces adsorbed a high density of nanowires. We have also found evidence of similar behavior for PIn/DNA nanowires. Samples were prepared for AFM by placing drops of PIn/DNA solution onto Si/SiO$_2$ substrates; these samples were taken at different times after the addition of oxidant to start the nanowire synthesis. Polymer wires of a range of diameters were observed (5−20 nm), and longer incubation times resulted in thicker wires (Figure 4). The AFM images also show evidence that the thicker structures comprise ropes of individual nanowires, as can be seen in cases where the ropes partially unravel (Figure 4d). We suggest the observation of rope-like structures will be quite general for DNA-templated polymer nanowires in which the charge on the DNA is compensated by the cationic conductive polymer. We also observe that, on hydrophilic surfaces, PIn/DNA nanowires form large, dense agglomerates, as in the polypyrrole/DNA system.

An interesting difference between the PIn/DNA and polypyrrole/DNA systems is that the PIn/DNA structures are smoother and their thickness is very uniform along the length of the nanowire after a reaction time of 24 h. To make a quantitative comparison, we measured the standard deviation of PIn/DNA and PPY/DNA nanowire heights along 5 μm lengths of nanowires at 10 evenly spaced intervals from tapping mode images. For each nanowire, we computed the fractional standard deviation by dividing by the mean height and then computed the mean and standard error for 8 similar
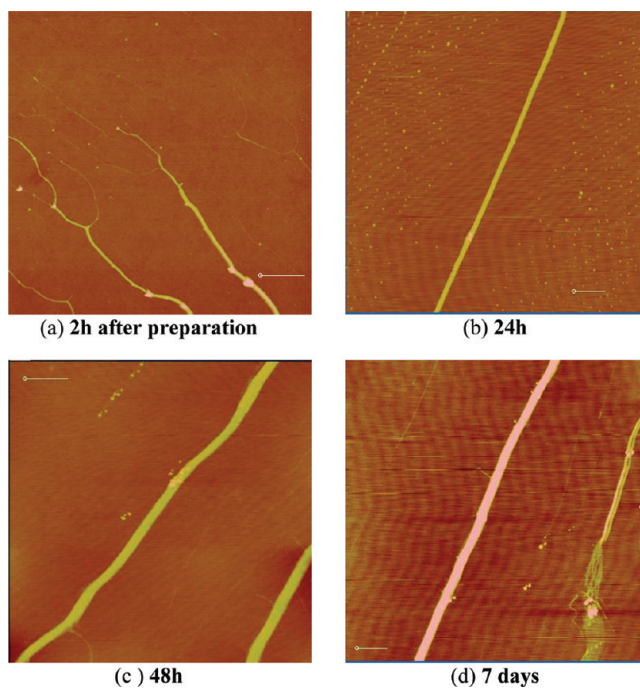

(a) **2h after preparation**

(b) **24h**

(c) **48h**

(d) **7 days**

Figure 4. Selection of AFM images of PIn/DNA nanowires on silanized SiO$_2$/Si surfaces showing the effect of reaction time on the height and width of the nanowires. (a) Nanowires observed 2 h after preparation, (b) after 24 h, (c) after 48 h, and (d) after 7 days. The formation of "frayed ends" by unraveling of the strands making up the nanowires is evident in image (d). The scale bar in all images is 1 μm, and the grayscale corresponds to a height range of (a) 15 nm, (b) 45 nm, and (c,d) 40 nm.

sized nanowires of each type; these wires were chosen to reflect the range of sizes observed (mean diameter ~15 nm, range 6−33 nm (PPY), 5−29 nm (PIn)) For PIn/DNA, we obtained a fractional standard deviation of 0.09 ± 0.03 and for PPY/DNA a larger value of 0.24 ± 0.14. The reason for this difference between the two polymers is unclear, but because the PIn nanowires are very regular, it allowed us to make a study of the effect of nanowire diameter on scanned conductance microscopy. In addition, we observe that dense agglomerates of nanowires formed on clean, hydrophilic Si/SiO$_2$ surfaces are surrounded by many individual wires that are stretched out from the main mass. This effect could be observed by AFM (Supporting Information) but is more easily seen in the wider field of view obtained in a fluorescence microscope (Figure 5).

Fluorescence Microscopy of PIn/DNA Cast on Si/SiO$_2$ Surfaces. Fluorescence imaging of the PIn nanowires was found to be straightforward, and the bright emission of these nanowires enabled us to image single nanowires in a standard epifluorescence apparatus. Figure 5 shows a fluorescence image of PIn/DNA cast from solution onto a Si/SiO$_2$ chip. The bright mass at the top of the image is a dense network of PIn/DNA that is typically observed for deposition on hydrophilic surfaces. As the solution dries, the meniscus recedes and individual nanowires appear stretched out around the periphery of the main mass. We suggest that this is an example of "molecular
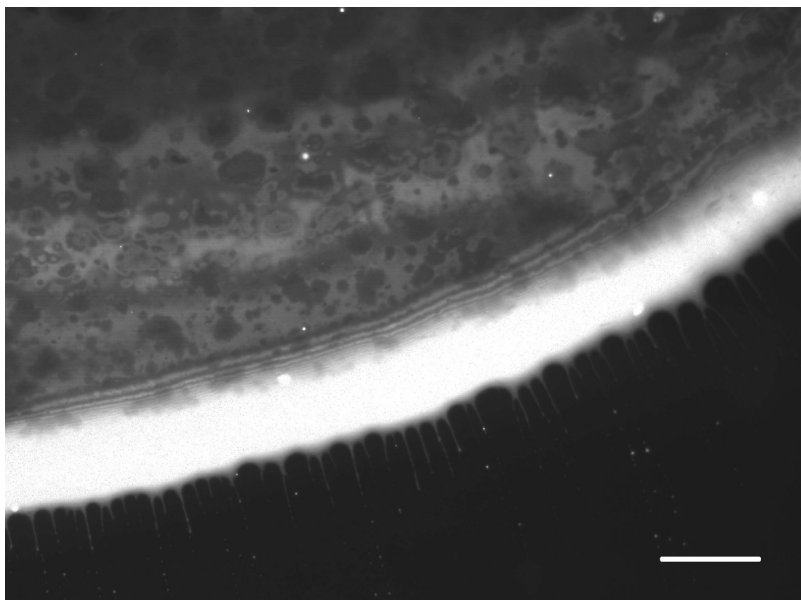
Figure 5. Fluorescence image of PIn/DNA nanowires on a Si substrate. The excitation light (Hg lamp) passed through a 300−400 nm band-pass filter with a maximum transmission of 65% at λ = 365 nm, and the emission was observed through a 420 nm long pass filter. The scale bar is 67 μm.

combing" in which the fluid motion and surface forces act to stretch DNA molecules.[35] The phenomenon is well-known for DNA, but we have also found that DNA-templated nanowires can also be combed in this manner.[13,14] In this work, we have found that the combination of fluorescence microscopy and the molecular combing effect facilitates the characterization of individual nanowires by conductive AFM. After casting a droplet of PIn/DNA solution onto a Si/SiO$_2$ chip and allowing the droplet to dry, a fluorescence image can easily be taken of a large section of the droplet to confirm the presence of single nanowires stretched out from the periphery of the main dry mass of PIn/DNA. We can then prepare an In/Ga eutectic contact to the main mass close enough to a suitable section of the periphery where stretched-out nanowires are present. After transfer to the AFM, this region can then be more easily identified in the optical image (an example is given in the Supporting Information) from the camera of the Nanoscope V/Dimension AFM. The AFM tip is then brought into contact with a single nanowire that is connected directly to the dense mass of PIn/DNA. In our c-AFM experiment, therefore, the large, dense network of nanowires serves as one contact to the nanowire we image and the conductive AFM tip forms the second contact. Below, we demonstrate that the measured conductance reflects dominantly the conductance of the nanowire protruding from the PIn/DNA mass and that the contribution of the PIn/DNA mass is negligible. We believe this procedure is a novel use of molecular combing in DNA-templated polymers and that it simplifies the task of making two electrical contacts to such a small object and allows us to distinguish the contact resistance from the nanowire intrinsic resistance by

making a series of measurements at different distances along the nanowire.

Electrical Characterization of PIn/DNA Nanowires: Conductive AFM. Conductive atomic force microscopy (c-AFM) techniques can provide direct electrical characterization as well as surface topography of individual nanowires through the use of a metallized tip to contact the nanowire. The main technical difficulty lies in making a second connection between the nanowire and the external circuit. In our c-AFM experiments, we selected a single PIn/DNA nanowire at the edge of a dense mass of nanowires on a hydrophilic SiO$_2$/Si substrate similar to that shown in Figure 5. The dense mass of nanowires served as one contact and was itself connected to the metallic chuck using a drop of In/Ga eutectic. The other electrical contact was the tip of a metal-coated cantilever; although the tip was located about 1 mm from the In/Ga contact, the main resistance in the circuit is the individual nanowire of about 10 μm protruding from the main deposit. The c-AFM images were recorded with a bias of 0.5 V applied between the cantilever and the metallic chuck. Essentially, zero current (<10 pA) was observed when the tip was above a clean area of Si/SiO$_2$, but currents on the order of magnitude of 10 nA were observed when the tip was in contact with the nanowire. After collecting an image, the closed loop positioning system of the Nanoscope V was used to touch the nanowire at defined points (indicated as red crosses in the inset of Figure 6) and an I−V curve was recorded over the range of −5 to 5 V. The slope of this I−V curve at zero bias was used to estimate the conductance of the circuit, and Figure 6 shows a plot of the resistance as a function of the relative distance, d, of the tip along the nanowire in the direction away from the massive deposit of PIn/DNA. We interpret the data of Figure 6 in terms of a simple series circuit comprising three resistances; R_{tip}, R_{ext}, and $R_{wire}(d)$. R_{tip} is the tip/nanowire contact resistance; R_{ext} is the resistance between the nanowire and the external circuit, and $R_{wire}(d)$ is the resistance of the portion of the nanowire between the tip and the main PIn/DNA deposit. The measured circuit resistance is clearly the sum of these, and we are assuming all of the distance dependence is in $R_{wire}(d)$.

Figure 6 shows that the circuit resistance increases in a roughly linear manner with d because the current must flow through a longer portion of the nanowire,
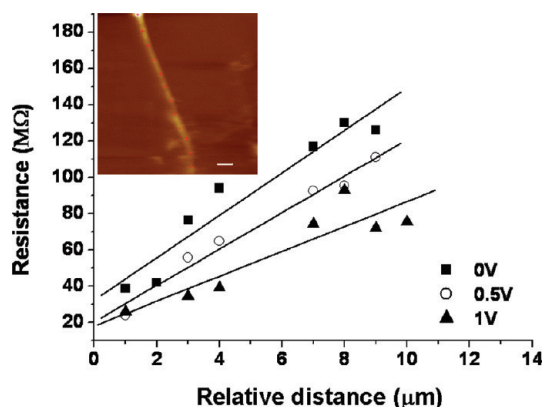
Figure 6. PIn/DNA nanowire resistance at zero bias as a function of tip-contact relative distance for different applied forces in single-point c-AFM $I-V$ measurements. The inset shows the AFM image of the nanowire acquired prior to the $I-V$ measurements. The scale bar is 1.1 μm, and several measurement positions are indicated by red crosses.

and $R_{\text{wire}}(d)$ is the largest resistance in the circuit. However, to make a quantitative analysis, it is necessary to evaluate also R_{tip} and R_{ext}. Figure 6 also shows the effect of increasing the tip/nanowire contact force by increasing the set point voltage from 0 to 1.0 V. A clear decrease in the intercept on the resistance axis is observed at higher forces, which is expected if R_{tip} rather than R_{ext} is the dominant contribution to this intercept. There is also a small apparent change in the slope of the least-squares regression lines, which is not expected on the basis of a simple series resistance model of the experiment. However, this effect is probably not statistically significant given the scatter in the data, and therefore, we do not try and interpret it quantitatively. The slope of the best fit lines gives the nanowire resistance per unit length = $1.0 \pm 0.2 \times 10^{11}$ Ω cm^{-1}. Using the diameter and width of the nanowire observed in the contact mode image (Figure 6, inset enlarged image in Supporting Information) to calculate the cross-section area (assumed elliptical), we were able to estimate the nanowire conductivity. The width of the nanowire is certainly overestimated due to tip-broadening effects, but this is partly compensated by the well-known tendency of height measurements to underestimate the diameter of DNA and related nanowires.[14] A more precise tip-broadening deconvolution procedure is probably not warranted because variations in doping density and defect level produce greater uncertainties. Nevertheless, we obtain an estimate of 2.5 ± 0.5 S cm^{-1} for the nanowire conductivity. This is significantly more conductive than bulk PIn ($10^{-2}-10^{-1}$ S cm^{-1}) but similar to the lower bound of 4 S cm^{-1} we reported previously for polypyrrole/DNA nanowires.[10]

Electrical Characterization of PIn/DNA Nanowires: Two-Terminal $I-V$ Characteristics and Temperature Dependence of the Conductance. In addition to the c-AFM technique above, we also prepared microfabricated Au electrodes on a thermally oxidized Si chip for direct two-terminal $I-V$ characterization of PIn/DNA nanowires. This method re-
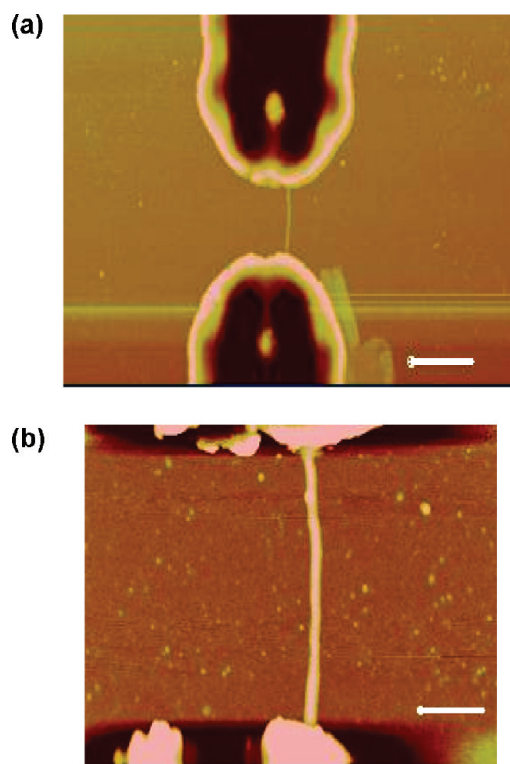

(a)

(b)

Figure 7. (a) Tapping mode AFM image of a PIn/DNA nanowire aligned across microfabricated Au electrodes. The mean nanowire diameter is 19 nm, and the interelectrode length is 1.7 μm. The grayscale (height) corresponds to 200 nm, and the scale bar is 2 μm. (b) Image of the same nanowire at higher resolution, showing the interelectrode gap region; the grayscale (height) is 35 nm, and the scale bar represents 500 nm.

lies on the possibility to align nanowires across the Au microelectrodes by molecular combing and is therefore less straightforward to implement than c-AFM but allows characterization of the temperature dependence of the conductance. Most conducting polymers show an increase in conductivity with temperature typical of hopping conductors; however, the precise nature of the temperature dependence might be affected by many factors such as the polymer structure, degree of crystallinity, and dimensionality. Characterization of this temperature dependence therefore provides valuable insight into the conduction mechanism of the PIn/DNA nanowires. Figure 7 shows a tapping mode AFM image of a PIn/DNA nanowire (thin white line in the center of the image) aligned between two Au electrodes (the depressions at the top and bottom of the image). The diameter of the nanowire was estimated as 19 nm from the height of this image. Figure 8 shows the $I-V$ curves for this nanowire recorded at a series of temperatures over the range of 233 to 373 K.

The $I-V$ curves are nonlinear, as we have previously observed for similar measurements on polypyrrole/DNA nanowires.[10,13] The reason for this behavior is most likely to be a small tunneling barrier at the Au/polymer contacts. Nevertheless, we can extract the conductance at zero bias (G) from the slope of the curves
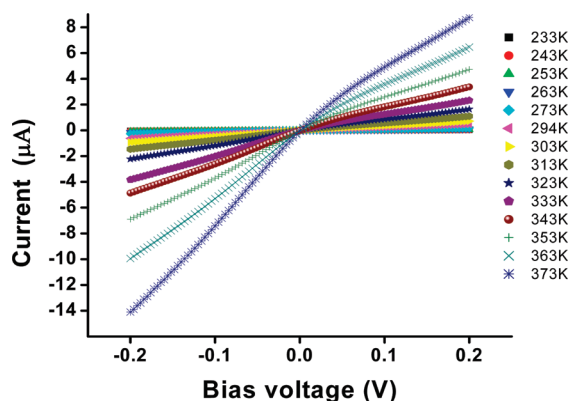
Figure 8. Current−voltage curves for the PIn/DNA nanowire of Figure 7. Each curve was recorded at a fixed temperature, and the full data set covers the temperature range of 233−373 K.

at 0 V and observe its temperature dependence. The temperature dependence of the conductivity of conjugated polymers has typically been fitted to expressions of the form $\ln G = \ln G_0 - (T_0/T)^\beta$, where the parameter β depends on the underlying theoretical model and also the dimensionality of the system. Thick films of conducting polypyrrole prepared chemically exhibit a temperature dependence described by 3D variable range hopping where $\beta = 1/4$.[36,37] Thin films conform to the Efros−Shklovskii model and $\beta = 1/2$,[38] although a transition to Arrhenius behavior above a critical temperature was observed.[39] A simple calculation extending the original variable range hopping model to 1D and 2D structures predicts $\beta = 1/(1 + D)$, that is, 1/2 for nanowires. However in 1D systems, the electron cannot avoid a large barrier and the conductance may be dominated by such "breaks": Arrhenius behavior ($\beta = 1$) is then expected.[40] A simple nearest neighbor hopping model also predicts $\beta = 1$. Figure 9 shows the corresponding Arrhenius plot of the conductance of the nanowire of Figure 7. The Arrhenius equation clearly describes the conductance data over the full range of temperatures accessible to us, and the fitted parameters
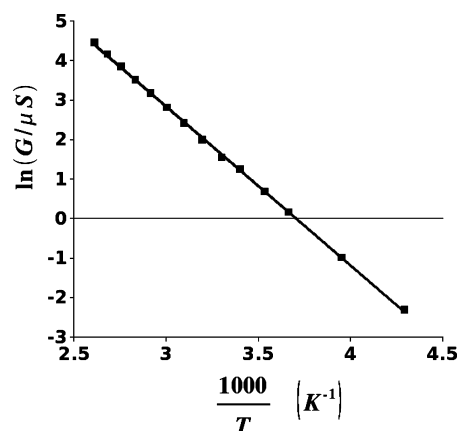
are $G_0 = 3.0 \pm 0.25$ S and $T_0 = 4025 \pm 24$ K or in terms of energy $E_a = 33.5 \pm 0.2$ kJ mol^{-1}.

At room temperature, the conductivity of the wire (using the height and width from the AFM image) is about 40 S cm^{-1}. This is larger than that determined from the c-AFM experiment (2.5 ± 0.5 S cm^{-1}), but this may reflect variations between and within samples due to doping levels and structural order (see scanned conductance microscopy data below). A wide range of local conductivities has also been observed in conductive polymer films by c-AFM.[41] Nevertheless, both the values for PIn/DNA nanowires are clearly greater than the conductivity of bulk polyindole ($10^{-2}-10^{-1}$ S cm^{-1}).[19,23,24] Similar values have, however, been observed for chemically prepared polypyrrole.[37,42]

We also observed the repeatability of the conductance measurements using two cycles of heating and cooling (Supporting Information). No significant hysteresis was observed in the *G versus T* plots upon heating and cooling; the standard error of conductance measurements at any particular temperature was not greater than 5.1% and for most values of temperature was in fact about 1−2%. The observed conductance increase is therefore not due to chemical changes such as the evaporation of water, and the data also indicate the thermal stability of the PIn/DNA nanowire.

Electrical Characterization of PIn/DNA Nanowires: Contactless Measurements by Scanned Conductance Microscopy. In addition to direct two-terminal measurements, we also characterized the electrical properties of the PIn/DNA nanowires by a noncontact method called scanning conductance microscopy.[43,44] This technique provides a useful method to assess qualitatively the conduction pathways in nanoscale objects without the necessity of making numerous electrical contacts. Scanned conductance microscopy (SCM) is a variant of electric force microscopy (EFM) in which the phase of the tip motion is measured as a function of the dc bias between the tip and a conductive substrate (degenerately doped Si) coated with a dielectric layer (of SiO$_2$). When a conductive wire is inserted between the tip and the substrate, it changes the tip/substrate capacitance. This affects the energy stored in the capacitance, and the second derivative of this energy with respect to the height of the tip above the surface is equivalent to a change in the force constant of the cantilever.[43,44] The sign of this effect and therefore the sign of the phase shift as the tip passes over the wire depends on whether the wire is conductive or insulating. Insulating objects produce a positive phase shift dependent on their polarizability, but conductive wires show a negative phase shift. The magnitude of these phase shifts depends on the geometry of the wire, the height of the tip above the surface (lift height), and the square of the dc bias (*V*). During an EFM measurement, the main scan records the surface topographical data in tapping mode. In the subsequent interleave scan, the tip is lifted and kept at
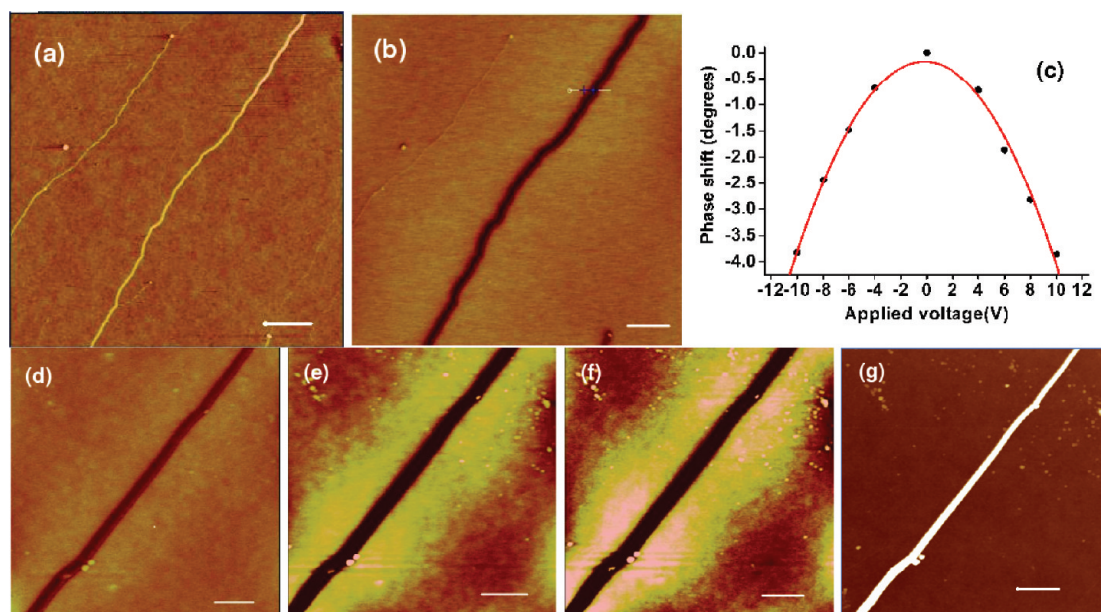

Figure 9. Arrhenius plot for the zero-bias conductance of the PIn/DNA nanowire in Figures 7 and 8. The fitted parameters are $E_a = 33.5 \pm 0.2$ kJ mol^{-1} and $G_0 = 3.0 \pm 0.25$ S.

Figure 10. AFM and scanned conductance (EFM phase) images of PIn/DNA nanowires on SiO$_2$/Si surface with a SiO$_2$ thickness of 220 nm. (a) AFM image of a nanowire with a diameter of 5 nm (grayscale 10 nm). (b) Phase image of the same nanowire at a tip/sample bias of −6 V and lift height of 60 nm. (c) Phase shift as a function of applied voltage of PIn/DNA nanowire with a diameter of 28 nm and a length of 9 μm aligned on a SiO$_2$/Si surface with a SiO$_2$ thickness of 220 nm; the lift height is 70 nm. (d−f) EFM phase images of the same nanowire show the phase angle of the tip oscillation at the following tip/sample biases: (d) +4 V, (e) +6 V, and (f) +10 V. (g) AFM height image of the nanowire in d−f. In all phase images, the grayscale corresponds to 3°, and the scale bar is 1 μm in all images.

fixed height above the surface, whose topography is obtained in the first scan; this minimizes possible confounding effects due to the topography. Since EFM is also sensitive to trapped charges, the quadratic variation of phase shift with bias voltage is a useful test that the data observed are due to conductance effects rather than trapped charge or topography.

Figure 10 shows an AFM image and several scanned conductance images of PIn/DNA nanowires at different applied dc potentials. The nanowires appear as dark lines in the scanned conductance images; this corresponds to a negative phase shift as the tip crosses the nanowire and demonstrates the existence of charge conduction in the wire. As a check on the origin of this effect, we plotted the phase shift against dc bias and observed the expected parabolic dependence of phase shift potential over the range from −10 to +10 V (Figure 10c). The absence of any significant linear dependence of phase shift on bias confirms that trapped charge makes no significant contribution to our data.[45]

Previous four-point probe studies of polypyrrole nanowires prepared by electrochemical synthesis in a porous alumina membrane have shown that the conductivity of polymer nanowires can vary substantially along their length.[46] A careful comparison of Figure 10a,b shows that the thinner wires in the top left and bottom right quadrants of the image show a weak positive phase shift (enlarged images in Supporting Information). This is characteristic of an insulating object and demonstrates that not all of the samples of PIn/DNA nanowires are conductive. One can also observe thin

branches leading off the nanowire running through the center of Figure 10a that are insulating by this test and also a defect that seems to terminate the end of the conductive portion of a wire in the bottom right of Figure 10b. However, we did observe that the thicker (>5 nm dia) wires showed a uniform negative phase shift along the portion of their length that was visible in a single image (Figure 10d−f).

The uniformity of these wires made it possible to study the effect of nanowire radius on the scanned conductance effect. The raw data (phase shift *versus* dc bias *V*, Supporting Information) were fitted with a quadratic in *V*, and the best fit coefficient of V^2 was compared with the predictions of the models of ref 44. This coefficient is equal to $(Q/2k)(\partial^2 C/\partial h^2)$, where *C* is the change in the tip/substrate capacitance in the presence of a nanowire, *h* is the lift height, *Q* is the quality factor, and *k* is the cantilever spring constant. The capacitance contribution can be evaluated by considering the nanowire as a metallic cylinder lying on top of a dielectric and ignoring end effects. Since the length of the nanowire *L* is larger than the scan size, we assume it is equal to the length of λ-DNA, 16 μm. However, a numerical calculation shows that, even if the nanowire were a factor of 10 longer, the effect on the computed values would be no more than 1%; this is because $L \gg R_{tip} = 15$ nm. Figure 11 shows the variation of the coefficient of V^2 with nanowire radius, where the solid line is a numerical calculation based on the model of ref 44.

The model agrees reasonably with experiment for the smaller nanowires, but for larger radii, the theory
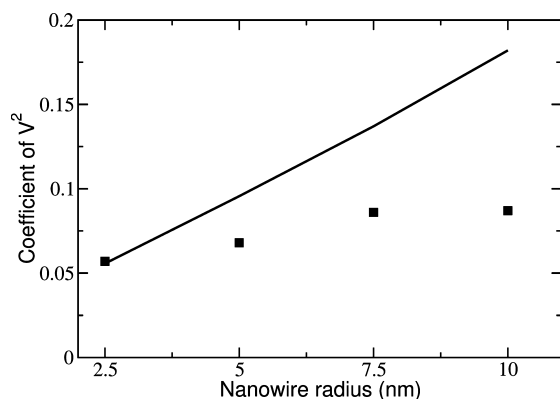
Figure 11. Coefficient of a quadratic fit to the plot of phase shift *versus* dc bias voltage (data in Supporting Information) against the nanowire diameter at a constant lift height of 60 nm. The squares represent experimental data, and the solid line is a numerical calculation based on the model of ref 44 for nanowires of various diameters on a SiO$_2$ dielectric (ε = 3.9) with a thickness of 220 nm, with a tip radius of 15 nm, a cantilever spring constant k = 5 N m^{-1} and Q = 250.

overestimates the scanned conductance effect. We suggest that this is due to the finite resistance of the nanowires and the dielectric properties of the nanowires themselves.

CONCLUSIONS

Continuous, smooth, and uniform PIn nanowires were chemically synthesized on a λ-DNA template by oxidation of indole with aqueous FeCl$_3$. FTIR, XPS, and UV−vis spectra confirm the formation of a supramolec-ular structure containing DNA and PIn. The electrical properties of the PIn/DNA nanowires were tested using EFM and c-AFM techniques as well as two-terminal I−V measurements at microfabricated Au electrodes. EFM imaging in the "scanned conductance" mode was a convenient method to demonstrate the conductivity of the PIn/DNA nanowires, and the smooth and uniform nature of these nanowires allowed us to confirm the predicted dependence of the phase shift on lift height, nanowire diameter, and applied voltage.[43,44] The room temperature (290 K) conductivity of the prepared PIn/DNA nanowires was estimated as 2.5 ± 0.5 S cm^{-1} by a c-AFM technique and about 40 S cm^{-1} from measurements made on a sample combed across the 1.7 μm gap between Au microelectrodes on SiO$_2$. The spread in the measured values can be attributed to variations in doping level and possible changes in the structural order of PIn/DNA nanowires. However, the conductivity of PIn/DNA is significantly higher than typical values for bulk PIn prepared by an analogous method (10^{-2}−10^{-1} S cm^{-1}).[23] Temperature-dependent I−V measurements using the Au microelectrode technique showed a simple Arrhenius behavior characteristic of a thermally activated process with an activation energy of 33.5 ± 0.2 kJ mol^{-1}. The conductance measurements during two heating/cooling cycles over the range of 233 to 373 K were also observed to be reproducible within 5.1%, which demonstrates the thermal stability of the PIn/DNA nanowires.

EXPERIMENTAL SECTION

Materials. Indole and other chemicals of AnalaR grade or equivalent were purchased from Sigma-Aldrich and used as received without any further purification. Lambda DNA (λ-DNA, 500 ng μL^{-1}) was purchased from New England Biolabs, cat no. N30011S (New England Biolabs (U.K.) Ltd. Hitchin, Herts. SG4 0TY United Kingdom). Calf thymus DNA was obtained from Sigma. All solutions were prepared in water from a Barnstead nanopure purification train with nominal resistivity of 18.2 MΩ · cm.

Methods. *Preparation and Alignment of PIn/DNA Nanowires.* PIn/DNA nanowires were chemically synthesized using FeCl$_3$ as an oxidant; 5 μL of freshly prepared indole solution (6.24 mM) was added to 20 μL of λ-DNA (500 ng μL^{-1}) in the presence of 5 μL of MgCl$_2$ (0.5 mM), then 5 μL of FeCl$_3$ (1 mM) was added dropwise into this solution. The solution was thoroughly mixed and allowed to react for at least 1 h at room temperature prior to analysis. PIn/DNA solution was deposited on Si and oriented by the molecular combing technique. In order to facilitate the alignment of nanowires on Si/SiO$_2$ substrates, the hydrophobicity of the SiO$_2$ was increased by treating the Si/SiO$_2$ substrates with chlorotrimethylsilane (Me$_3$SiCl) vapor for about 10 min.[13] Typically, 2−3 μL of PIn/DNA solution was dropped on the silanized Si/SiO$_2$ surface and combed, then removed with a micropipet or by wicking with filter paper.

Characterization. *FTIR Spectroscopy.* For FTIR measurements, about 8 μL of PIn/DNA solution was deposited on a clean Si(100) substrate and left to dry for 1 h prior to measurements. FTIR spectra (64 co-added and averaged scans) in the range from 600 to 4000 cm^{-1} were recorded in absorbance mode by using a Bio-rad FTS-40 spectrometer operating with 4 cm^{-1} spectral resolu-tion and equipped with a liquid-nitrogen-cooled MCT detector. A clean Si(100) chip served as the background.

UV−Vis Spectroscopy. The UV−vis absorption spectra (wavelength range from 250 to 550 nm) were recorded on a Thermo-Spectronic GENESYS 6 spectrophotometer at room temperature. For UV−vis measurements, PIn/DNA solution was made using calf thymus DNA (CT-DNA). Typically, 0.125 mL of 6.24 mM freshly prepared indole solution was added to 0.5 mL of CT-DNA solution (162.5 μg mL^{-1}, 10 mM Tris-HCl pH 8 + 1 mM EDTA) in the presence of 0.5 mM MgCl$_2$. Then, 0.125 mL of FeCl$_3$ (1 mM) was added dropwise to the solution. The mixture was stirred and allowed to react at room temperature for 1 h. PIn solution was prepared by the same process without CT-DNA as a control: the color of the solution was observed to become a light green upon addition of oxidant.

X-ray Photoelectron Spectroscopy. A Kratos Axis Ultra 165 photoelectron spectrometer equipped with a monochromic Al Kα X-ray excitation source (1486.7 eV) with an operating power of 150 W (15 kV, 10 mA) was used to collect photoemission spectra of PIn/DNA samples. The chamber pressure was 3.2 × 10^{-9} Torr. The photoelectrons were filtered by the hemispherical analyzer and recorded by multichannel detectors. For the survey scan, the pass energy was 20 eV and the step size was 0.3 eV. Some higher resolution spectra were recorded with a pass energy of 5 eV and a step size of 0.1 eV. The binding energies obtained in the XPS analysis were calibrated using Au$_{4f}$ (84.0 eV) as a reference. Photoemission spectra were fitted with a combination of mixed singlet components using the Winspec program. Backgrounds were subtracted by the Shirley method.[47] PIn/DNA samples were prepared for XPS by depositing 3 μL of solution on a clean Si(100) substrate and then left to dry in air at room temperature in a laminar flow hood to minimize contamination (Model VLF

ARTICLE

4B, Envair, Haslingden, Lancs, U.K.) before being inserted into the chamber.

Fluorescence Microscopy. Fluorescence images were collected on an Axioplan 2 microscope (Zeiss) using Axiovision Viewer 3 software (Zeiss). The fluorescence was excited using the light from a Hg lamp passed through a 300−400 nm band-pass filter with a maximum transmission of 65% at λ = 365 nm. The emitted light was separated from scattered light using a long pass filter with a cutoff at 420 nm.

Probe Microscopy. Samples for atomic force microscopy (AFM) and electrostatic force microscopy (EFM) were prepared by combining 2−3 μL of PIn/DNA solution on 1 cm^2 SiO$_2$/Si substrates at room temperature and then allowing it to dry for 1 h. All of the AFM images are height images unless otherwise indicated. The SiO$_2$ thickness was about 220 nm, as determined by a spectrometric thin film analyzer (Filmetrics F40). All of the AFM imaging was performed in air on a Dimension Nanoscope V (Veeco Inc., Metrology group) using NanoProbe tips (Veeco Inc.). Vibrational noise was reduced with an isolation system (Manfrotto).

For EFM and c-AFM measurements, we used MESP probes (n-doped Si cantilevers, with a Co/Cr coating, Veeco Inc.). These probes are 200−250 μm long, with a resonant frequency of about 79 kHz, a quality factor (Q) between 200 and 260, and a spring constant between 1 and 5 N m^{-1}. In EFM measurements, an independently controlled bias was used to create an electrostatic field between the tip and the sample (the tip was grounded, while the bias was applied at the sample). The images reported show the phase of the tip oscillation at a set lift height (50−90 nm typical) above the surface. In this mode, EFM has also been referred to as scanning conductance microscopy (SCM) because the phase is related to the force gradient and is sensitive to the conductance of nanowires as well as their polarizability.

For conductive AFM (c-AFM) measurements, a constant bias was also applied between the tip and the sample (the tip was grounded). Electrical contact was made by applying a drop of In/Ga eutectic to one corner of the chip and to the metallic chuck. c-AFM imaging was performed in contact mode, with an applied bias of 0.5 V. The imaged area was about 1 mm away from the In/Ga contact. The closed loop system of the Dimension V instrument makes it possible to reproducibly position the tip at a point of interest identified in the image of the PIn/DNA nanowire and to record I−V measurements at that point. The resistance was estimated from the reciprocal of the slope of the I−V curve at zero bias.

Two-Terminal Current−Voltage Characterization of PIn/DNA Nanowires. Two-terminal conductivity measurements were performed using gold electrodes deposited on clean oxidized silicon. First, an appropriate mask was prepared with eight pairs of large pads and small fingers and patterned using a reverse photolithography process on the clean substrate. Next, reactive ion etching was used to make a 100 nm deep trench in a 220 nm thick SiO$_2$ dielectric; this reduces the step height at the boundary between the gold electrodes and the oxide gap in the final device and facilities alignment of polymer nanowires across the gap. The trench was filled with e-beam-evaporated metals (10 nm Cr adhesion layer followed by 90 nm Au). Next, a lift-off process was used to remove unwanted Cr and Au. The gap between each pair of fingers ranged from one to several micrometers, and the two pads in each pair are separated by 80 μm. The two small gold fingers in each pair provide contacts to the DNA-templated PIn wires, and the two large gold pads serve as electrical contacts for external measurement of the system.

Prior to aligning the PIn/DNA nanowires, the oxide layer was treated with Me$_3$SiCl vapor to produce a hydrophobic surface between the metal electrodes to facilitate molecular combing. A 2 μL drop of an aqueous solution of PIn/DNA nanowires was placed on these electrodes and aligned across the gap between the Au fingers by molecular combing.

Electrical measurements were made using a probing station (Cascade Microtech) and a B1500A semiconductor analyzer (Agilent). For each of the electrical tests, the current was measured for applied voltages from −10 to 10 V in steps of 0.05 V. All of the electrical measurements were carried out in air without light illu-

mination. I−V curves at various temperatures were performed on the probe station using a thermal chuck system (Model ETC-200 L, ESPEC, Japan).

Supporting Information Available: FTIR assignments, additional AFM and scanned conductance microscopy data, and thermal cycling data for the two-terminal I−V measurements at microfabricated Au electrodes. This material is available free of charge *via* the Internet at http://pubs.acs.org.

REFERENCES AND NOTES

1. Wang, Y.; Mirkin, C. A.; Park, S.-J. Nanofabrication beyond Electronics. *ACS Nano* **2009**, *3*, 1049–1056.
2. Houlton, A.; Pike, A. R.; Galindo, M. A.; Horrocks, B. R. DNA-Based Routes to Semiconducting Nanomaterials. *Chem. Commun.* **2009**, 1797–1806.
3. Storm, A. J.; van Noort, J.; de Vries, S.; Dekker, C. Insulating Behavior for DNA Molecules between Nanoelectrodes at the 100 nm Length Scale. *Appl. Phys. Lett.* **2001**, *79*, 3881–3883.
4. Cai, L.; Tabata, H.; Kawai, T. Self-Assembled DNA Networks and Their Electrical Conductivity. *Appl. Phys. Lett.* **2000**, *77*, 3105–3106.
5. Braun, E.; Eichen, Y.; Sivan, U.; Ben-Yoseph, G. DNA-Templated Assembly and Electrode Attachment of a Conducting Silver Wire. *Nature* **1998**, *391*, 775–778.
6. Seidel, R.; ColombiCiacchi, L.; Weigel, M.; Pompe, W.; Mertig, M. Synthesis of Platinum Cluster Chains on DNA Templates: Conditions for a Template-Controlled Cluster Growth. *J. Phys. Chem. B* **2004**, *108*, 10801–10811.
7. Richter, J.; Mertig, M.; Pompe, W.; Monch, I.; Schackert, H. K. Construction of Highly Conductive Nanowires on a DNA Template. *Appl. Phys. Lett.* **2001**, *78*, 536–538.
8. Monson, C. F.; Woolley, A. T. DNA-Templated Construction of Copper Nanowires. *Nano Lett.* **2003**, *3*, 359–363.
9. Patolsky, F.; Weizmann, Y.; Lioubashevski, O.; Willner, I. Au-Nanoparticle Nanowires Based on DNA and Polylysine Templates. *Angew. Chem., Int. Ed.* **2002**, *41*, 2323–2327.
10. Dong, L.; Hollis, T. A.; Connolly, B. A.; Wright, N. G.; Horrocks, B. R.; Houlton, A. DNA-Templated Semiconductor Nanoparticle Chains and Wires. *Adv. Mater.* **2007**, *19*, 1748–1751.
11. Wang, L.; Wei, G.; Qi, B.; Zhou, H.; Liu, Z.; Song, Y.; Yang, X.; Li, Z. Electrostatic Assembly of Cu$_2$O Nanoparticles on DNA Templates. *Appl. Surf. Sci.* **2006**, *252*, 2711–2716.
12. Kundu, S.; Lee, H.; Liang, H. Synthesis and Application of DNA−CdS Nanowires within a Minute Using Microwave Irradiation. *Inorg. Chem.* **2008**, *48*, 121–127.
13. Pruneanu, S.; Farha Al-Said, S. A.; Dong, L.; Hollis, T. A.; Galindo, M. A.; Wright, N. G.; Houlton, A.; Horrocks, B. R. Self-Assembly of DNA-Templated Polypyrrole Nanowires: Spontaneous Formation of Conductive Nanoropes. *Adv. Funct. Mater.* **2008**, *18*, 2444–2454.
14. Dong, L.; Hollis, T. A.; Fishwick, S.; Connolly, B. A.; Wright, N. G.; Horrocks, B. R.; Houlton, A. Synthesis, Manipulation and Conductivity of Supramolecular Polymer Nanowires. *Chem.—Eur. J.* **2007**, *13*, 822–828.
15. Li, X.; Wan, M.; Li, X.; Zhao, G. The Role of DNA in PANI-DNA Hybrid: Template and Dopant. *Polymer* **2009**, *50*, 4529–4534.
16. Farha Al-Said, S. A.; Hassanien, R.; Hannant, J.; Galindo, M. A.; Pruneanu, S.; Pike, A. R.; Houlton, A.; Horrocks, B. R. Templating Ag on DNA/Polymer Hybrid Nanowires: Control of the Metal Growth Morphology Using Functional Monomers. *Electrochem. Commun.* **2009**, *11*, 550–553.
17. Jennings, P.; Jones, A. C.; Mount, A. R. Fluorescence Properties of Electropolymerised 5-Substituted Indoles in Solution. *J. Chem. Soc., Faraday Trans.* **1998**, *94*, 3619–3624.
18. Weiqiang, Z.; Jingkun, X.; Mengping, G. The Fluorescence Spectra of Polyindole and Its Derivatives. *Chem. Bull. Huaxue Tongbao* **2008**, *71*, 75–79.

19. Billaud, D.; Maarouf, E. B.; Hannecart, E. Electrochemical Polymerization of Indole. *Polymer* **1994**, *35*, 2010–2011.

20. Billaud, D.; Maarouf, E. B.; Hannecart, E. Chemical Oxidation and Polymerization of Indole. *Synth. Met.* **1995**, *69*, 571–572.

21. A Zotti, G.; Zecchin, S.; Schiavon, G.; Seraglia, R. B.; Berlin, A.; Canavesi, A. Structure of Polyindoles from Anodic Coupling of Indoles: An Electrochemical Approach. *Chem. Mater.* **1994**, *6*, 1742–1748.

22. Saraç, A. S.; Ozkara, S.; Sezer, E. Electrocopolymerization of Indole and Thiophene: Conductivity-Peak Current Relationship and *In Situ* Spectroelectrochemical Investigation of Soluble Co-Oligomers. *Int. J. Polym. Anal. Charact.* **2003**, *8*, 395–409.

23. Tüken, T.; Yazici, B.; Erbil, A. Electrochemical Synthesis of Polyindole on Nickel-Coated Mild Steel and Its Corrosion Performance. *Surf. Coat. Technol.* **2005**, *200*, 2301–2309.

24. Eraldemir, O.; Sari, B.; Gok, A.; Unal, H. I. Synthesis and Characterization of Polyindole/Poly(vinyl acetate) Conducting Composites. *J. Macromol. Sci., Part A* **2008**, *45*, 205–211.

25. Waltman, R. J.; Diaz, A. F.; Bargon, J. Substituent Effects in the Electropolymerization of Aromatic Heterocyclic-Compounds. *J. Phys. Chem.* **1984**, *88*, 4343–4346.

26. Jennings, P.; Jones, A. C.; Mount, A. R.; Thomson, A. D. Electrooxidation of 5-Substituted Indoles. *J. Chem. Soc., Faraday Trans.* **1997**, *93*, 3791–3797.

27. Billaud, D.; Humbert, B.; Thevenot, L.; Thomas, P.; Talbi, H. Electrochemical Properties and Fourier Transform-Infrared Spectroscopic Investigations of the Redox Behaviour of Poly(indole-5-carboxylic acid) in $LiClO_4$−Acetonitrile Solutions. *Spectrochim. Acta, Part A* **2003**, *59*, 163–168.

28. Ryu, K. S.; Park, N. G.; Kim, K. M.; Lee, Y. G.; Park, Y. J.; Lee, S. J.; Jeong, C. K.; Joo, J.; Chang, S. H. The Physicochemical Properties of Polyindole/Thiol Composites. *Synth. Met.* **2003**, *135*−*136*, 397–398.

29. Talbi, H.; Maarouf, E. B.; Humbert, B.; Alnot, M.; Ehrhardt, J. J.; Ghanbaja, J.; Billaud, D. Spectroscopic Studies of Electrochemically Doped Polyindole. *J. Phys. Chem. Solids* **1996**, *57*, 1145–1151.

30. An, S.; Abdiryim, T.; Ding, Y.; Nurulla, I. A Comparative Study of the Microemulsion and Interfacial Polymerization for Polyindole. *Mater. Lett.* **2008**, *62*, 935–938.

31. Lee, C.-Y.; Gong, P.; Harbers, G. M.; Grainger, D. W.; Castner, D. G.; Gamble, L. J. Surface Coverage and Structure of Mixed DNA/Alkylthiol Monolayers on Gold: Characterization by XPS, NEXAFS, and Fluorescence Intensity Measurements. *Anal. Chem.* **2006**, *78*, 3316–3325.

32. Briones, C.; Mateo-Marti, E.; Gómez-Navarro, C.; Parro, V.; Román, E.; Martín-Gago, J. A. Ordered Self-Assembled Monolayers of Peptide Nucleic Acids with DNA Recognition Capability. *Phys. Rev. Lett.* **2004**, *93*, 208103.

33. Eaves, J. G.; Munro, H. S.; Parker, D. An ESCA Study of Polypyrrole Oxidation. *Polym. Commun.* **1987**, *28*, 38.

34. Carquigny, S.; Sanchez, J.-B.; Berger, F.; Lakard, B.; Lallemand, F. Ammonia Gas Sensor Based on Electrosynthesized Polypyrrole Films. *Talanta* **2009**, *78*, 199–206.

35. Bensimon, D.; Simon, A. J.; Croquette, V.; Bensimon, A. Stretching DNA with a Receding Meniscus: Experiments and Models. *Phys. Rev. Lett.* **1995**, *74*, 4754–4757.

36. Joo, J.; Lee, J. K.; Lee, S. Y.; Jang, K. S.; Oh, E. J.; Epstein, A. J. Physical Characterization of Electrochemically and Chemically Synthesized Polypyrroles. *Macromolecules* **2000**, *33*, 5131–5136.

37. Chakrabarti, S.; Banerjee, D.; Bhattacharyya, R. Enhancement of Room Temperature Electrical Conductivity of Polypyrrole by Chemical Modification. *J. Phys. Chem. B* **2002**, *106*, 3061–3064.

38. Efros, A. L.; Shklovskii, B. I. Coulomb Gap and Low-Temperature Conductivity of Disordered Systems. *J. Phys. C* **1975**, *8*, L49–L51.

39. Bufon, C. C. B.; Heinzel, T. Transport Properties of Chemically Synthesized Polypyrrole Thin Films. *Phys. Rev. B* **2007**, *76*, 245206.

40. Fogler, M. M.; Teber, S.; Shklovskii, B. I. Variable-Range Hopping in Quasi-One-Dimensional Electron Crystals. *Phys. Rev. B.* **2004**, *69*, 035413.

41. Lee, H. J.; Park, S.-M. Electrochemistry of Conductive Polymers 37. Nanoscale Monitoring of Electrical Properties during Electrochemical Growth of Polypyrrole and Its Aging. *J. Phys. Chem. B* **2005**, *109*, 13247–13254.

42. Winther-Jensen, B.; Chen, J.; West, K.; Wallace, G. Vapor Phase Polymerization of Pyrrole and Thiophene Using Iron(III) Sulfonates as Oxidizing Agents. *Macromolecules* **2004**, *37*, 5930–5935.

43. Bockrath, M.; Markovic, N.; Shepard, A.; Tinkham, M.; Gurevich, L.; Kouwenhoven, L. P.; Wu, M. S. W.; Sohn, L. L. Scanned Conductance Microscopy of Carbon Nanotubes and λ-DNA. *Nano Lett.* **2002**, *2*, 187–190.

44. Staii, C.; Johnson, A. T.; Pinto, N. J. Title: Quantitative Analysis of Scanning Conductance Microscopy. *Nano Lett.* **2004**, *4*, 859–862.

45. Jespersen, T. S.; Nygard, J. Charge Trapping in Carbon Nanotube Loops Demonstrated by Electrostatic Force Microscopy. *Nano Lett.* **2005**, *5*, 1838–1841.

46. Shen, J. Y.; Chen, Z. J.; Wang, N. L.; Yan, H. L.; Shi, G. Q.; Jin, A. Z.; Gu, C. Z. Electrical Properties of a Single Electrochemically Template-synthesized Polypyrrole Nanowire. *Appl. Phys. Lett.* **2006**, *88*, 253106.

47. Shirley, D. A. High-Resolution X-ray Photoemission Spectrum of Valence Bands of Gold. *Phys. Rev. B* **1972**, *5*, 4709.